

1 **Scattering of guided waves at delaminations in composite plates**

2 **Bibi I.S. Murat <sup>a)</sup>, Pouyan Khalili <sup>b)</sup>, and Paul Fromme <sup>a)</sup>**

3 *<sup>a)</sup> Department of Mechanical Engineering, University College London, WC1E 7JE, UK*

4 *<sup>b)</sup> Department of Mechanical Engineering, Imperial College London, SW7 2AZ, UK*

5

6 **Email:** p.fromme@ucl.ac.uk

7

8 **Running title:** Guided Wave Scattering at Delaminations

9

10 **7<sup>th</sup> April 2016**

11 **Abstract**

12 Carbon fiber laminate composites are increasingly employed for aerospace structures as they  
13 offer advantages, such as a good strength to weight ratio. However, impact during the  
14 operation and servicing of the aircraft can lead to barely visible and difficult to detect damage.  
15 Depending on the severity of the impact, fiber and matrix breakage or delaminations can  
16 occur, reducing the load carrying capacity of the structure. Efficient nondestructive testing  
17 and structural health monitoring of composite panels can be achieved using guided ultrasonic  
18 waves propagating along the structure. The scattering of the  $A_0$  Lamb wave mode at  
19 delaminations was investigated using a full three-dimensional (3D) Finite Element (FE)  
20 analysis. The influence of the delamination geometry (size and depth) was systematically  
21 evaluated. In addition to the depth dependency a significant influence of the delamination  
22 width due to sideways reflection of the guided waves within the delamination area was found.  
23 Mixed-mode defects were simulated using a combined model of delamination with localized  
24 material degradation. The guided wave scattering at cross-ply composite plates with impact  
25 damage was measured experimentally using a non-contact laser interferometer. Good  
26 agreement between experiments and FE predictions using the mixed-mode model for an  
27 approximation of the impact damage was found.

28

29

30 **PACS numbers:** 43.40.Fz, 43.35.Zc, 43.35.Cg, 43.40.Le

31

32 **Keywords:** Lamb Waves, Composites, Impact Damage, Finite Element (3D FEA)

33

## 34 I. INTRODUCTION

35 The usage of composite materials in aerospace structures has increased significantly as they  
36 offer significant advantages such as an excellent strength to weight capacity. However, the  
37 combination of carbon fibers and epoxy matrix in typical carbon-fiber reinforced polymer  
38 (CFRP) pre-preg composites is susceptible to impact loading. Low-velocity impact can  
39 induce barely visible damage<sup>1</sup>, including matrix cracking, delamination, and fiber breakage,  
40 that can reduce the integrity of the structure<sup>2</sup>. Evidence of extensive delamination in the  
41 region adjacent to the impact zone has been shown<sup>3</sup> and it was found that this could reduce  
42 the overall load bearing capacity by up to 80%<sup>4</sup>. In contrast to matrix cracks or fiber breakage,  
43 delamination can occur in the absence of any visible surface damage, making it difficult to  
44 detect by visual inspection<sup>5</sup>. Therefore, it is important to efficiently monitor the composite  
45 structure during its service life to detect such damage and to ensure the safe operation of the  
46 structure. Guided ultrasonic waves (GUW) have the potential for the efficient nondestructive  
47 monitoring of large structures, as they can propagate over considerable distances at low  
48 excitation frequencies. This could significantly reduce the inspection time for large structures  
49 and be employed as part of a structural health monitoring (SHM) system<sup>6,7</sup>.

50

51 However, the scattering of guided waves by delaminations in a composite plate is a complex  
52 problem<sup>8</sup>. The propagation characteristics of the guided waves are complicated due to the  
53 anisotropic and inhomogeneous properties of the composites<sup>9,10</sup>. Together with typically  
54 high attenuation values for CFRP, this makes monitoring and inspection using higher guided  
55 wave modes difficult and only limited work has been reported<sup>11</sup>. Typically it has been found  
56 to be advantageous to operate with a single wave mode at low frequency in order to avoid

57 complications in the signal analysis and high attenuation<sup>1</sup>. The fundamental symmetric mode  
58  $S_0$  has attractive properties, as at low frequency it has limited dispersion and the fastest  
59 propagation velocity. However, the velocity depends strongly on the propagation direction  
60 relative to the composite layup fiber direction and the  $S_0$  mode is typically coupled with the  
61  $SH_0$  mode<sup>12</sup>. Furthermore, it has been reported that the  $S_0$  mode is not sensitive to  
62 delaminations between plies being under zero shear stress condition<sup>13</sup>. Recently significant  
63 effort has been focused on the fundamental anti-symmetric mode  $A_0$ , which has a shorter  
64 wavelength than the  $S_0$  mode<sup>14</sup> and thus in principle better sensitivity for defect detection.  
65 Furthermore, the directionality of the wave propagation characteristics is significantly less  
66 dependent on the anisotropic material properties, leading to similar velocities in all directions  
67 for quasi-isotropic and cross-ply (0/90) layups<sup>12</sup>.

68

69 The  $A_0$  mode has been employed to detect different types of damage, such as cracking,  
70 fatigue and delaminations in composite structures<sup>15</sup>. It has been demonstrated that the  $A_0$   
71 mode tends to be more sensitive to delaminations than the  $S_0$  mode and can detect  
72 delaminations at any depth<sup>16</sup>. Mode conversion from the  $A_0$  to  $S_0$  mode was observed when  
73 the guided wave interferes with the delamination boundaries<sup>17</sup>, confirmed from experimental  
74 work<sup>18</sup>. Delaminations can in principle be located by estimating the propagation speed and  
75 time of flight from the reflected signal<sup>19</sup>. It was found that separate reflections from the  
76 delamination edges appear when the delamination length increases (relative to the  
77 wavelength)<sup>20</sup>. Work was performed on composites subjected to impact damage<sup>21, 22</sup>. From  
78 numerical simulations to characterize the scattering pattern generated at a circular

79 delamination, it was found that the amplitudes around the delamination showed a large  
80 forward scattered wave relative to the reflected pulse<sup>8</sup>.

81

82 Numerical models have been developed to characterize impact damage on composite plates,  
83 mostly employing 2D FE models of wave propagation and scattering in composites<sup>13, 17, 23</sup>.

84 It was also observed that there is no converted  $S_0$  mode when the  $A_0$  mode encounters  
85 delaminations located at a symmetric interface. The combination of several damage  
86 mechanisms for realistic impact damage in laminated composites makes the accurate  
87 modelling more challenging, with limited studies employing full 3D analysis<sup>24</sup>. Recent  
88 work<sup>25</sup> has demonstrated that 3D simulations can accurately predict the scattering  
89 characteristics of guided waves at a circular-shaped delamination. The directivity pattern of  
90 the scattered  $A_0$  wave mode around a defect representing cracking in the composite materials,  
91 modeled as a 3D conical shape with reduced material properties, has been predicted<sup>26</sup>. Impact  
92 damage was characterized using an X-ray computed tomography scan of a damaged  
93 composite sample and used as the basis for a numerical model implementing the complex 3D  
94 delamination geometry to investigate the interaction of guided waves with impact damage<sup>27</sup>.

95

96 The focus of this contribution is the understanding of the interaction of the  $A_0$  guided wave  
97 mode with delaminations, and a systematic study of the influence of the delamination size  
98 (length and width) and depth on the wave scattering was conducted using 3D FE simulations.  
99 Scattering of the  $A_0$  guided wave mode at impact damage was observed experimentally, with  
100 increased amplitude at the impact location, and a repeatable scattering pattern with significant

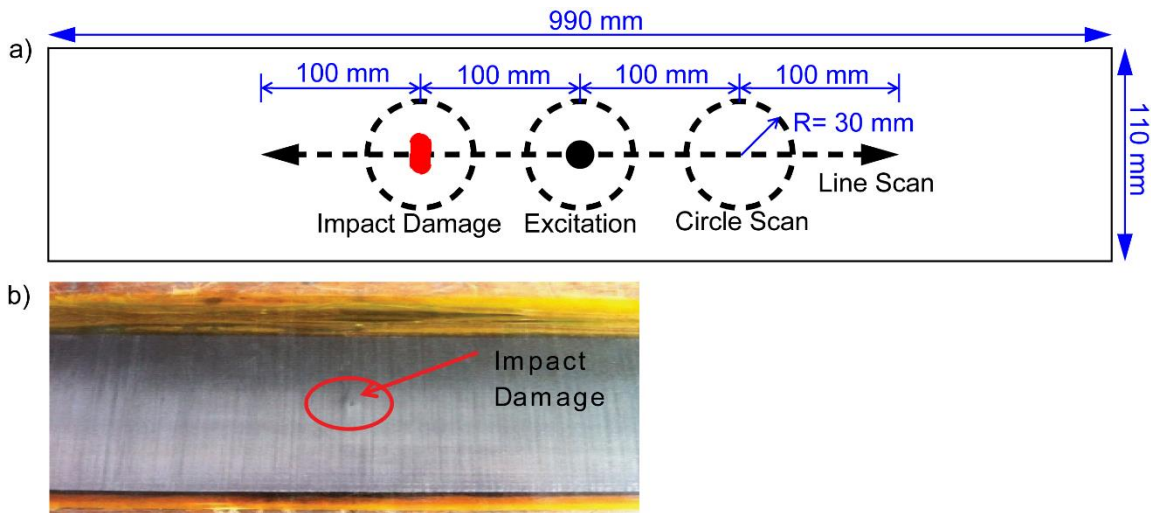
101 amplitude reduction of the guided wave propagating past the damage location<sup>28</sup>. Multi-mode  
102 impact damage was modelled as an additional reduction of material stiffness and the  
103 predicted wave scattering was compared to experimental results for impact damage.

104

## 105 **II. EXPERIMENTAL GUIDED WAVE MEASUREMENT OF IMPACT DAMAGE**

106 Two specimens were supplied by the Composite Systems Innovation Centre, University of  
107 Sheffield, which had been investigated in a separate study<sup>29</sup>. The composite plates (990 mm  
108 x 110 mm x 2 mm) were fabricated with unidirectional pre-pregs by autoclave cure using  
109 Cytec 977-2 / Tenax HTS cross-ply laminates (Fig. 1a). The plates consist of 8 pre-preg  
110 layers with a symmetric layup sequence of  $[0/90]_{2s}$ . Additionally, the plates contain a 25  $\mu\text{m}$   
111 thick polyimide film and an 18  $\mu\text{m}$  thick layer of flexible printed circuit boards for electrical  
112 resistance measurements<sup>29</sup>. The specimens had been subjected to a 7.4 J impact damage using  
113 a hemispherical 15 mm impactor head and following standard drop weight impact  
114 procedures. A small degree of fiber fracture and indentation was visible on the surface of the  
115 plates (Fig. 1b). For one of the plates a standard ultrasonic C-scan had shown an extensive  
116 delamination around the impact location<sup>30</sup>. A piezoelectric transducer to excite the  $A_0$  guided  
117 wave mode, consisting of a piezoelectric disc (Ferroperm Pz27, 5 mm diameter, 2 mm  
118 thickness) and a brass backing mass (5 mm diameter, 6 mm height), was glued onto the plate  
119 with Loctite 2-part epoxy 100 mm from the center of the impact damage. The excitation  
120 signal was a 5 cycle sinusoidal tone burst modulated by a Hanning window with a center  
121 frequency of 100 kHz, generated in a programmable function generator and amplified to  
122 about 200 Vpp. The velocity of the out-of-plane displacement was measured using a laser  
123 vibrometer fixed to a scanning rig and moved parallel to the specimen. The time traces of the

124 received signals were filtered using a band-pass filter (4<sup>th</sup> order Butterworth, cut-off  
125 frequencies 75 – 125 kHz) and were recorded and averaged (20 averages) using a digital  
126 storage oscilloscope. All signals were saved to a PC and further analyzed using Matlab. The  
127 maxima of the signal envelopes were obtained using Hilbert transform and evaluated. Two  
128 types of scans were performed; (i) horizontal line scans over a length of 200 mm from the  
129 transducer location in both directions with 1 mm step size; and (ii) circular scans with 30 mm  
130 radius measured every 5° around the excitation location, impact damage, and a symmetrically  
131 located undamaged area. Measurements on the undamaged part of the specimens were  
132 performed as a baseline measurement and to study the wave propagation characteristics of  
133 the A<sub>0</sub> Lamb wave mode in the undamaged composite plates for comparison to the FE  
134 simulations.



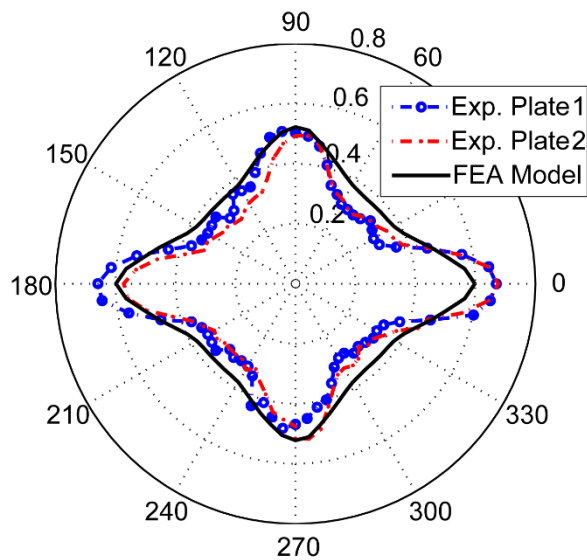
135  
136 **Figure 1:** a) Schematic of cross-ply plates and measurement locations (not to scale);  
137 b) photo of specimen with barely visible impact damage (marked).  
138  
139

### 140 **III. FINITE ELEMENT MODEL**

141 The full 3D FE model of a large, layered composite plate with dimensions of 1000 mm  
142 x 1000 mm x 2 mm was defined using a program in MATLAB to specify the model and  
143 damage parameters. The description of the 8 individual layers with the same lay-up as the  
144 experimental specimens ( $[0/90]_{2s}$ ) was implemented. The individual layers were modeled  
145 according to material properties of a unidirectional composite plate<sup>10</sup>. Rayleigh damping was  
146 set to  $\beta = 30$  ns to match the guided wave attenuation measured for the undamaged part of  
147 the composite specimens. Element size of 1 mm in the x- and y- directions (along the plate)  
148 and 0.25 mm in the z-direction (one element per layer through thickness) was employed,  
149 resulting in 8 million elements to model the plate. The element type was chosen as an 8-node  
150 linear brick element with reduced integration (C3D8R). The employed element size and time  
151 step fulfill the usual stability criteria of at least 10 elements per wavelength<sup>31</sup>. The wave  
152 propagation in the undamaged plate was verified against theoretical predictions and was  
153 found to be accurate (e.g., simulation phase velocity within 1% of theoretical value predicted  
154 using Disperse software<sup>32</sup>).

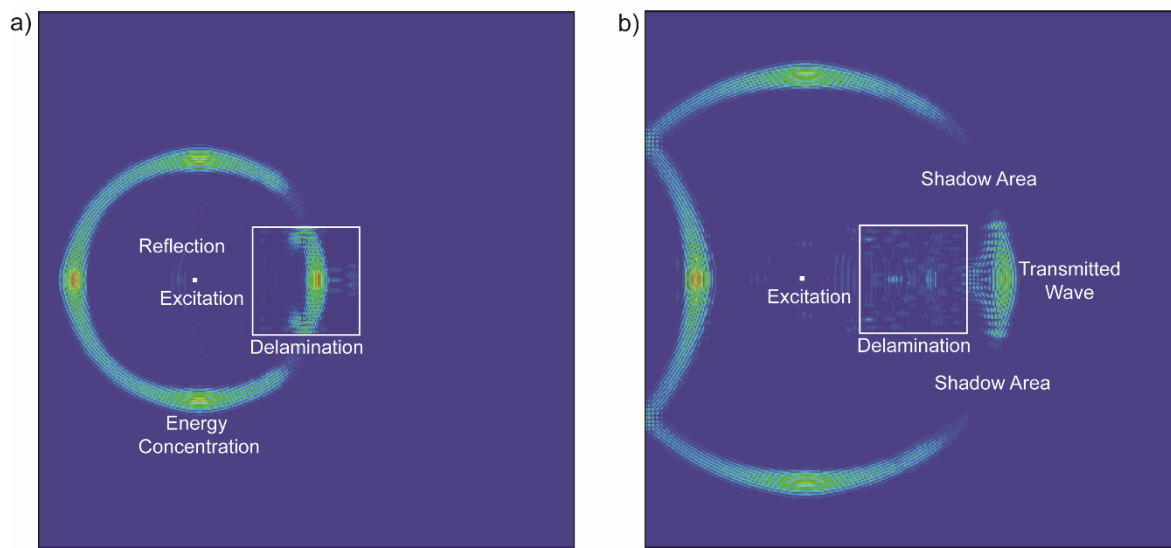
155 An additional layer of FE nodes along the delaminated area with the same co-ordinates, but  
156 not connected to the coinciding nodes, was created. Two separated layers of elements were  
157 thus defined, connected to the respective nodes along the delaminated area. This simulates  
158 two free surfaces which do not interact and represents a zero-volume delamination. Both  
159 rectangular and circular delamination shapes were modeled, approximating the circular shape  
160 with the Cartesian grid. The size (length and width) of the delamination was varied in the  
161 range of 10 mm to 50 mm, and the depth of delamination was changed in 0.25 mm steps.

162 Additionally a large delamination (200 mm x 200 mm) at 1 mm depth and an undamaged  
163 plate as the baseline case were modelled. For the investigation of multi-mode defects, the  
164 delamination was placed at 0.5 mm and 1 mm depth and a matching area of reduced stiffness  
165 properties (25%, 50%, and 75% reduction) through the thickness was modelled. Out-of-plane  
166 excitation was introduced as a point force to selectively generate an  $A_0$  Lamb wave  
167 propagating along the plate<sup>33,34</sup>. The excitation signal consisted of a 5 cycle sinusoidal tone  
168 burst modulated by a Hanning window, as for the experiments. The excitation location was  
169 placed 100 mm from the center of the delamination to match the experimental setup (200  
170 mm for large delamination model). The out-of-plane displacement was monitored at the same  
171 locations as for the line and circular scans performed experimentally. For the circular scans  
172 the signal was interpolated between the 4 adjacent nodes around the monitoring location.  
173 Hilbert transform was used to extract the maximum of the signal envelopes for each  
174 monitoring node. Additionally the incident wave pulse was monitored on the matching nodes  
175 of the baseline simulation for the undamaged plate. The amplitude of the scattered wave was  
176 isolated by subtracting the time traces and recording the maximum amplitude of the envelope  
177 of the difference signal.



178

179 **Figure 2** (color online): Comparison between experimental results for 2 plate specimens  
 180 and FE simulations for amplitude circular scan (30 mm radius) around excitation location;  
 181 100 kHz center frequency.



182

183 **Figure 3** (color online): FE simulation of guided wave stress field (von Mises): a) 200  $\mu$ s;  
 184 b) 360  $\mu$ s; 200 mm x 200 mm rectangular delamination (1 mm depth); 100 kHz center  
 185 frequency.

## 186 **IV. RESULTS AND DISCUSSION**

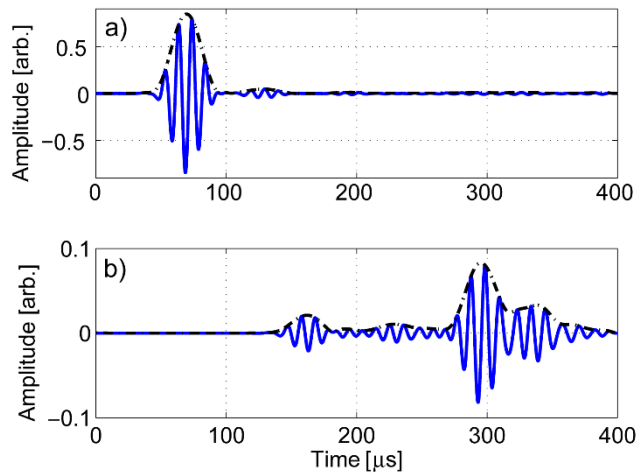
### 187 **A. Interaction with a large delamination**

188 To validate the FE simulations, the amplitude of the excited  $A_0$  mode pulse on a circle around  
189 the excitation location was compared between the measurements for the 2 composite  
190 specimens and the FE simulations. Figure 2 shows the expected amplitude pattern with higher  
191 amplitude along the  $0^\circ$  and  $90^\circ$  fiber directions. Good repeatability of the amplitude pattern  
192 for the two composite specimens and a good general agreement with the prediction from the  
193 FE simulation can be observed. Due to the symmetric lay-up of the cross-ply plate the top  
194 and bottom outer layers are both in the  $0^\circ$  direction and lead to slightly higher bending  
195 stiffness in this direction. This can be seen to result in slightly higher amplitude in the  $0^\circ$   
196 direction compared to the  $90^\circ$  direction. The FE simulations predict slightly higher amplitude  
197 at  $45^\circ$  directions to the fiber orientation and slightly underestimates the amplitude increase  
198 in the  $0^\circ$  direction, but matches the experimental pattern overall well.

199 The interaction of an incident  $A_0$  wave mode with a large square delamination (200 mm x  
200 200 mm) positioned at the symmetrical plane (1 mm depth) of the 2 mm thick cross-ply  
201 composite plate was simulated. Figure 3a shows the snapshot at 200  $\mu$ s as the incident  $A_0$   
202 mode has propagated into the delamination area. As expected, the amplitudes of the excited  
203 wave are higher in the  $0^\circ$  and  $90^\circ$  fibre directions and a small entry reflection from the  
204 delamination can be observed. Ahead of the main  $A_0$  pulse on top of the delamination a mode  
205 converted  $S_0$  pulse can be observed with higher propagation velocity. As the delamination is  
206 symmetric through the depth only the  $A_0$  mode propagates in the undamaged plate. A  
207 sideways reflection of the  $A_0$  mode at the upper and lower boundaries of the delamination  
208 can be observed due to the lower acoustic impedance of the delamination area (reduced

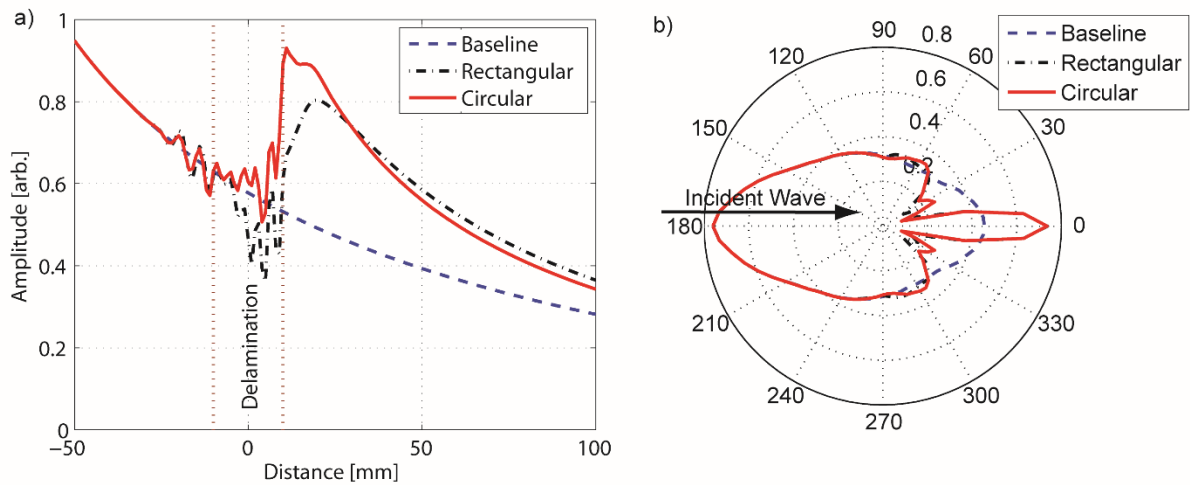
209 thickness). This leads to a shadow area with lower amplitude next to the delamination. This  
210 can be observed more clearly from the second time snapshot at 360  $\mu\text{s}$  in Fig. 3b. The  
211 transmitted  $A_0$  pulse has high amplitude in the horizontal direction with a shadow area with  
212 lower amplitudes above and below. A significant trapping of the wave due to reflections  
213 inside the delamination area can also be observed. Experimental observations<sup>35</sup> confirmed  
214 such multiple reflections leading to high wave energy on top of the delamination, which could  
215 serve as a marker for localizing defects.

216 Figure 4a shows the time trace monitored between the excitation and delamination locations.  
217 A reflected wave pulse at 110  $\mu\text{s}$  can be observed with about 10% of the amplitude of the  
218 incident wave pulse at 44  $\mu\text{s}$ . In principle the time difference can be used to approximately  
219 localize the delamination entry<sup>19</sup>. However, combined with the attenuation and beam spread,  
220 the entry reflection has rather low amplitude, limiting the practical detection range in  
221 composites. Figure 4b shows the time trace recorded behind the delamination (forward  
222 scattering). The arrival time of the largest transmitted wave pulse at 270  $\mu\text{s}$  corresponds to  
223 the main transmitted  $A_0A_0A_0$  wave group (propagating as  $A_0$  mode across the delamination).  
224 The arrival of the  $A_0S_0A_0$  wave group (propagating as  $S_0$  mode across the delamination) is  
225 observed earlier at 140  $\mu\text{s}$ , due to the higher velocity of the  $S_0$  mode across the large  
226 delamination<sup>17</sup>. Multiple reflected  $S_0$  pulses can also be observed between the  $A_0S_0A_0$  and  
227  $A_0A_0A_0$  pulses, with small amplitudes. This wave group keeps reflecting at the delamination  
228 boundaries and for the symmetrical delamination is confined to the delamination area. For  
229 large delaminations the faster transmitted wave pulse could serve as an indicator of a  
230 delamination, as the arrival time difference correlates to the delamination length.



231

232 **Figure 4** (color online): FE simulation of guided wave time signals for a 200 mm x 200  
 233 mm rectangular delamination (1 mm depth); a) 40 mm before delamination, b) 40 mm  
 234 behind delamination; 100 kHz center frequency.



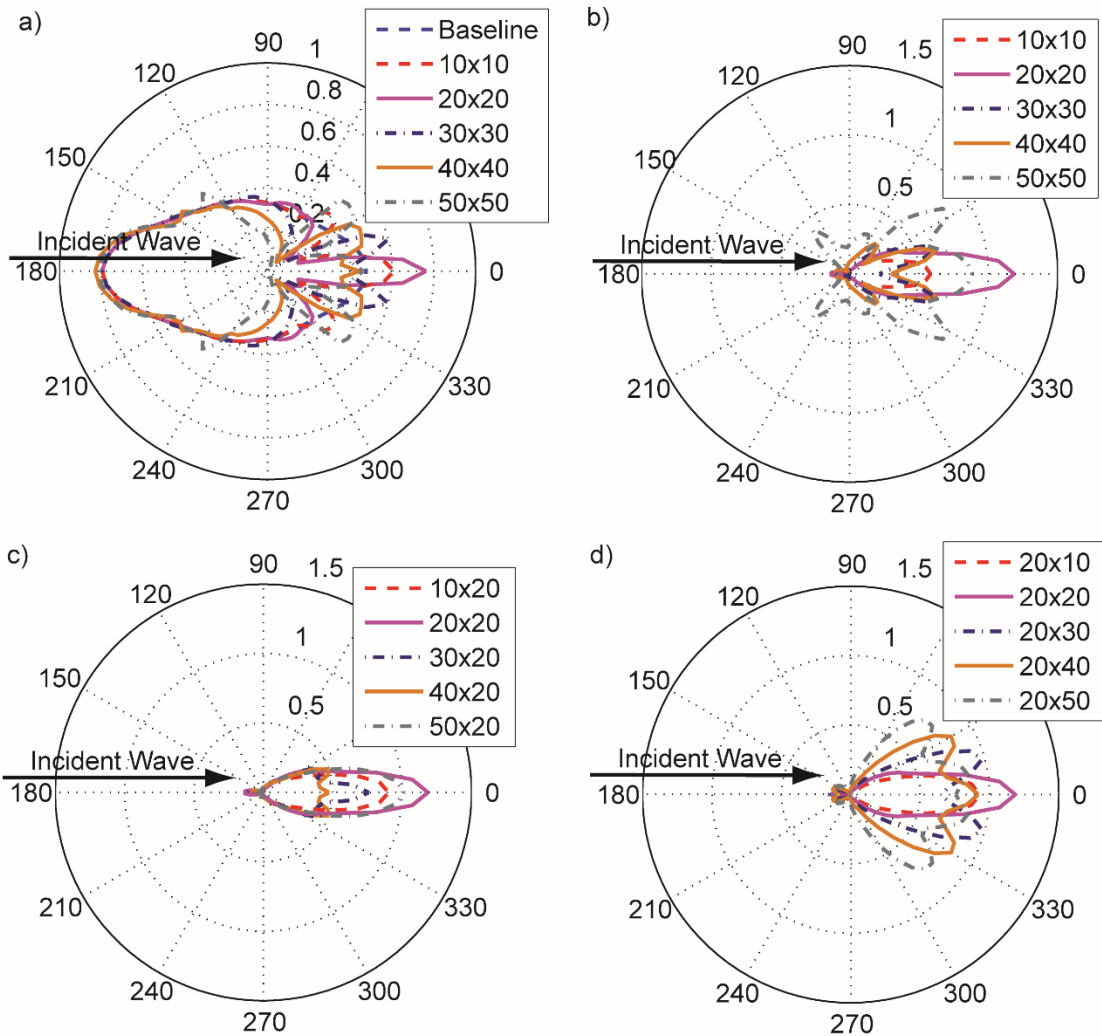
235

236 **Figure 5** (color online): FE simulations for scattering at different delamination shape;  
 237 baseline, rectangular delamination (20 mm x 20 mm); circular delamination (20 mm  
 238 diameter); a) amplitude across defect area; b) amplitude circular scan; 100 kHz center  
 239 frequency; 1 mm delamination depth.

240

241 **B. Influence of delamination shape**

242 In practice impact leads to irregularly shaped damage patterns, with delaminations often  
243 observed to have an approximately oval shape<sup>3</sup>. In this section it is considered whether a  
244 simple rectangular delamination shape can be used, which is straight-forward to implement  
245 in a FE model. Two regular shapes to represent a delamination are investigated: a rectangular-  
246 shaped delamination (dimensions: 20 mm x 20 mm) and a circular-shaped delamination  
247 (diameter: 20 mm). As can be seen from Fig. 5, both models resulted in comparable  
248 amplitude patterns, especially for the forward propagating wave. The peak amplitudes close  
249 to the circular shaped delamination (Fig. 5a) were seen to be slightly higher compared to the  
250 peaks from the square shaped delamination, and small differences in the angular scattering  
251 pattern were observed, particularly in the 30° and 330° directions (Fig. 5b), due to the  
252 different shapes causing slightly different scattering in these directions. It was observed that  
253 the circular and rectangular shaped delaminations of the same maximum extent (diameter  
254 matching rectangle) resulted in overall very similar scattering patterns and amplitudes. This  
255 confirms that the maximum length and width of the delamination are expected to have an  
256 influence on the guided wave scattering. Therefore, a simple and easy to implement  
257 rectangular shape was chosen for further FE modeling and analysis.



258

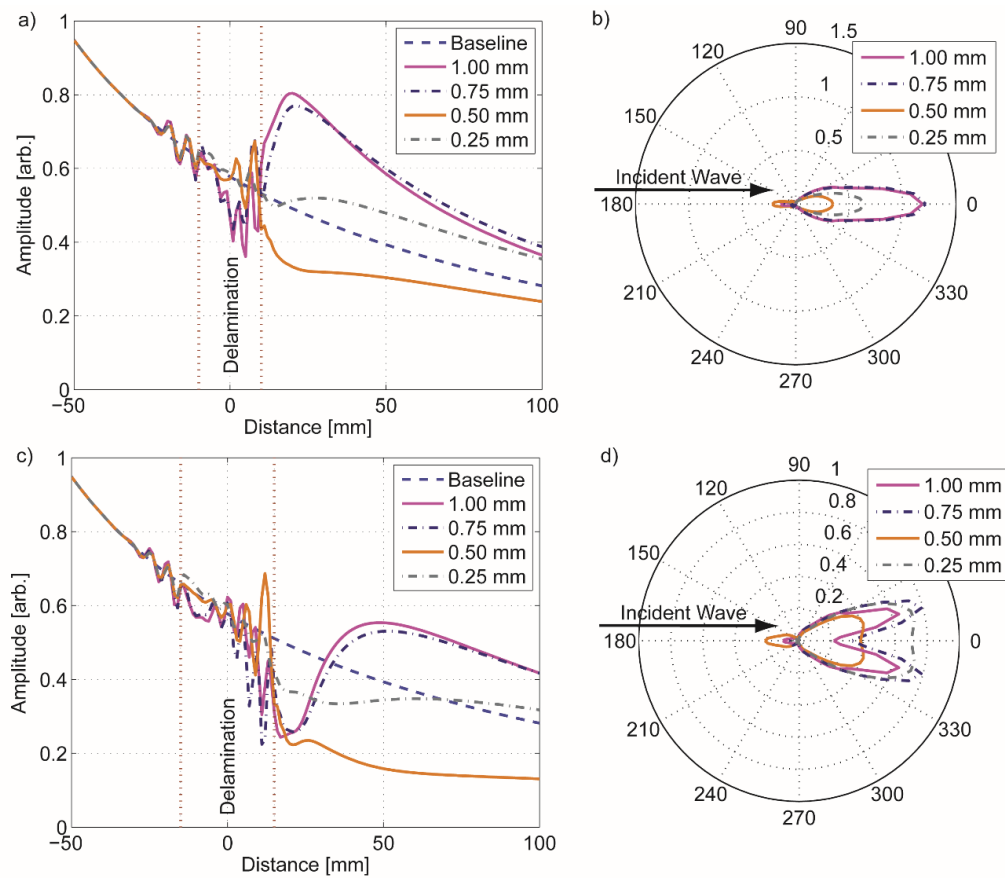
259 **Figure 6** (color online): FE simulations for scattering at different delamination sizes (1 mm  
 260 depth); a) amplitude circular scan (square delaminations); b) scattered difference amplitude  
 261 circular scan (square delaminations); c) scattered difference amplitude circular scan (varied  
 262 delamination length); d) scattered difference amplitude circular scan (varied delamination  
 263 width); 100 kHz center frequency; delamination dimensions in mm.

264

### 265 **C. Influence of delamination size**

266 The angular amplitude pattern of the  $A_0$  mode scattered at square delaminations with varying  
267 size at depth 1 mm can be seen in Fig. 6a. The backward scattered amplitudes (around  $180^\circ$ )  
268 show a regular pattern similar to the baseline data. Different forward scattering patterns can  
269 be observed at angles between  $270^\circ$  and  $90^\circ$ . For small delamination sizes (10 mm x 10 mm,  
270 20 mm x 20 mm) comparable to the wavelength of the  $A_0$  mode (15 mm) a large amplitude  
271 in the  $0^\circ$  direction and a reduced amplitude up to about  $\pm 30^\circ$  can be observed. For larger  
272 delamination sizes the forward scattering forms side lobes which, with increasing  
273 delamination size, move away from the main forward direction ( $0^\circ$ ), and a smaller forward  
274 amplitude is seen. Amplitude reduction for a wider range in the sideways direction up to  
275 about  $90^\circ$  for the largest considered delamination size (50 mm x 50 mm) was found. The  
276 amplitude of the scattered wave was isolated by subtracting the incident time traces from the  
277 baseline FE simulation and recording the maximum amplitude of the envelope of the  
278 difference signal (Fig. 6b). Forward scattering around the  $0^\circ$  direction was observed for the  
279 smallest considered delamination size (10 mm x 10 mm), increasing in magnitude for the 20  
280 mm x 20 mm delamination. For this case the complex magnitude in the  $0^\circ$  direction is larger  
281 than the baseline amplitude as the forward scattered wave is out of phase with the baseline  
282 case (due to the change in propagation velocity across the thinner sub-lamina of the  
283 delamination). As the delamination size increases further, the scattered amplitude side lobes  
284 move away from the  $0^\circ$  direction, leading to the scattering pattern observed in Fig. 6a. In  
285 order to separate the influence of the delamination length and width, two sets of simulations  
286 were performed, varying these independently from 10 mm to 50 mm. As shown in Fig. 6c  
287 the angular scattering pattern for a symmetrically located delamination is almost independent

288 of the delamination length with mostly only changes in the forward scattering amplitude ( $0^\circ$ ).  
289 No clear pattern of the magnitude of the forward scattering was found, as different  
290 delamination lengths lead to different phase changes compared to the propagation in the  
291 undamaged plate (baseline). Interestingly, there is a small back scattered amplitude ( $180^\circ$   
292 direction) for delamination lengths larger than 20 mm. This could be related to a reduced  
293 interference between reflections from the entrance and the exit of delaminations due to the  
294 increasing time delay, as has been observed in the case of a large delamination model<sup>20</sup>. Fig.  
295 6d shows the influence of the delamination width on the angular scattering pattern. For  
296 delamination sizes larger than the wavelength of the  $A_0$  mode, side lobes form and move  
297 away from the  $0^\circ$  direction with increasing delamination size. Based on the observations for  
298 the large delamination (Fig. 3), the directivity of the side lobes is related to the wave  
299 reflection at the sides of the delamination and energy trapping within the delamination. The  
300 geometry of the shadowed area at the delamination sides matches the angular directivity seen  
301 in Fig. 6d and can be approximated from geometric considerations (Fig. 3). This implies that  
302 the distance between the wave source (excitation) and the delamination has an influence on  
303 the observed scattering pattern, especially for the defect located close to the source, and  
304 should be taken into consideration for SHM applications<sup>34</sup>. The delamination width therefore  
305 has an important influence on the angular scattering pattern, as well as on the forward  
306 scattered amplitude, which cannot be captured using 2D FE simulations and should be  
307 considered using 3D FE simulations.



308

309 **Figure 7** (color online): FE simulations for scattering at different delamination depth and  
 310 size; a) amplitude across defect area (20 mm x 20 mm); b) scattered difference amplitude  
 311 circular scan (20 mm x 20 mm); c) amplitude across defect area (30 mm x 30 mm); d)  
 312 scattered difference amplitude circular scan (30 mm x 30 mm); 100 kHz center frequency.

313

#### 314 **D. Influence of delamination depth**

315 The influence of the delamination depth on the mode conversion and forward scattering has  
 316 been previously investigated from 2D FE simulations<sup>13, 17, 33</sup>. The scattered waves around  
 317 square 20 mm x 20 mm and 30 mm x 30 mm delaminations placed at different depths were  
 318 investigated. For both delamination sizes amplitude variations in the line scans can be seen  
 319 in front and on top of the delamination due to the interference of the incident and reflected

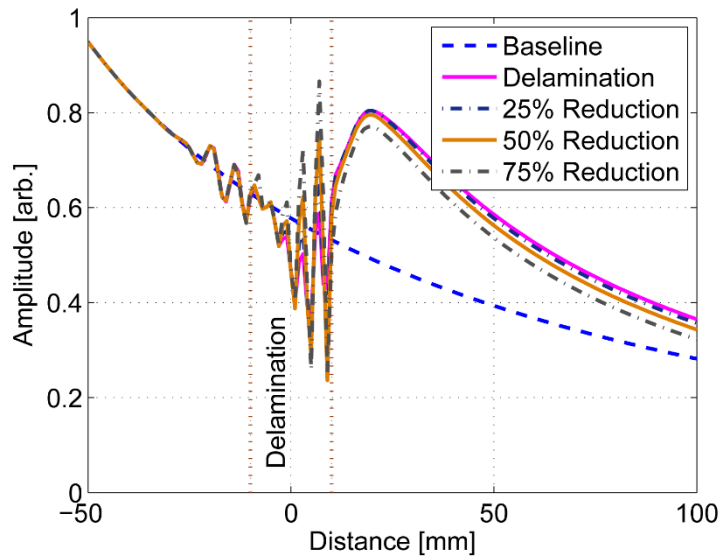
320 waves with only a small influence of the delamination depth (Fig. 7a/c). The effect of the  
321 delamination depth can be observed at the amplitude patterns behind the delamination region.  
322 The amplitudes of transmitted guided wave pulses past the delaminations located towards the  
323 center of the plate (0.75 mm and 1 mm depth) show a similar behaviour with an increase in  
324 amplitude due to the sideways reflection and energy trapping (Fig. 3). In contrast, for all case  
325 studies of different delamination sizes located at 0.50 mm depth an amplitude drop behind  
326 the delamination region was observed. When the delamination was located close to the plate  
327 surface (0.25 mm depth), the amplitude pattern can be seen to be close to the baseline data  
328 with limited change of the transmitted amplitudes. Using the baseline subtraction method,  
329 Fig. 7b/d shows the angular pattern of the isolated wave scattering. The scattering around  
330 delaminations at 0.75 mm and 1 mm depth close to the middle of the plate show similar  
331 behaviour with forward (20 mm x 20 mm) or side (30 mm x 30 mm) lobes of high amplitude  
332 (as observed in Fig. 6). The similar height of the sub-lamina on top and below the  
333 delamination for these cases leads to similar propagation velocities and acoustic impedances,  
334 and thus similar scattering patterns. For the case of the delamination placed close to the  
335 surface, i.e., 0.25 mm depth, Fig. 7b/d shows different magnitudes for the two delamination  
336 sizes as these lead to different phase shifts across the delamination. However, the change in  
337 amplitude of the transmitted waves for this depth was small (Fig. 7a/c). A different forward  
338 scattering pattern can be observed when the delamination is located at 0.50 mm depth with a  
339 consistent forward scattered wave leading to an amplitude drop in the line scans behind the  
340 delamination (Fig. 7a/c). The significant difference between wave speeds in the upper and  
341 lower sub-plates due to the unequal thicknesses of the sub-laminates contributes to the higher  
342 acoustic mismatch, leading to increased reflections and phase differences. This reduced

343 forward scattered wave amplitude was observed as well for all other investigated  
344 delamination sizes at a depth of 0.5 mm, but not necessarily for other delamination depths. It  
345 thus has to be concluded that, for the regular delamination shape considered here, both either  
346 increased or decreased forward scattered amplitude of the  $A_0$  wave mode can occur  
347 depending on the depth and size of the delamination and needs to be taken into consideration  
348 when devising damage detection algorithms for a SHM system.

349

#### 350 **E. Influence of reduction in material properties**

351 As low-velocity impact has been shown to induce distributed microscopic fibre breaking and  
352 matrix cracking<sup>3</sup>, and thus a local decay in the stiffness properties, a multi-mode defect  
353 consisting of a delamination with additional reduced stiffness properties was modelled<sup>26</sup>.  
354 Figure 8 shows a comparison of three FE models with a delamination and different material  
355 degradation compared to the model with only a delamination of 20 mm x 20 mm at 1 mm  
356 depth. It can be seen that there are increased amplitude peaks on the defective region for the  
357 three models with locally reduced stiffness. Since the wave velocity depends on the stiffness  
358 properties, a local change in the wave propagation velocity and thus an increased acoustic  
359 impedance mismatch occurs. This leads to an increase of the trapped energy and thus  
360 recorded wave amplitude with larger stiffness reductions. No significant influence of the  
361 stiffness property reduction on the angular scattering pattern was observed. In the region  
362 behind the defective area (Fig. 8), increasing stiffness reduction leads to a small drop in the  
363 forward scattered amplitude, but the overall influence on the guided wave scattering was  
364 found to be limited.



365

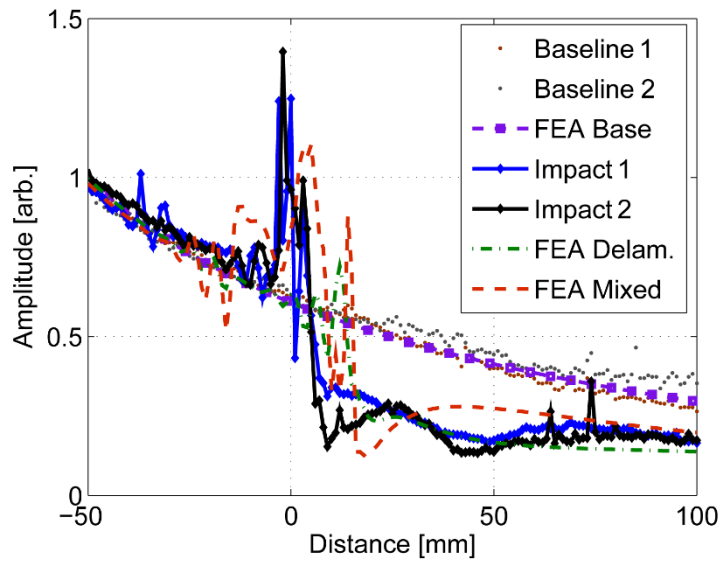
366 **Figure 8** (color online): FE simulations for baseline, delamination (20 mm x 20 mm, 1 mm

367

depth) and mixed-mode defect (delamination and 25%, 50%, 75% local material

368

degradation); amplitude across defect area; 100 kHz center frequency.



369

370 **Figure 9** (color online): Comparison between experimental results (baseline and impact

371

damage for 2 plates) and FE simulations for delamination (30 mm x 30 mm, 0.5 mm depth)

372

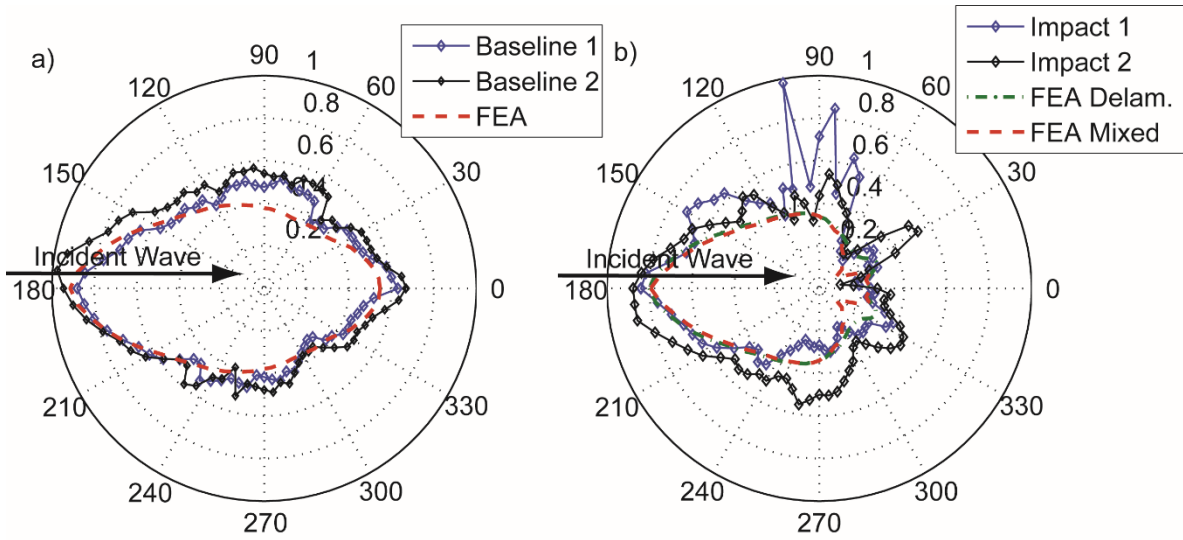
and mixed-mode defect (delamination and 75% material degradation); amplitude across

373

defect area; 100 kHz center frequency.

## 374 **V. COMPARISON TO MEASURED SCATTERED FIELD AT IMPACT DAMAGE**

375 Based on the observed scattering and the available information about the size and depth of  
376 the impact damage in the composite plates<sup>28, 30</sup>, a comparison was made between the  
377 experimental measurements and FEA results for a delamination size of 30 mm x 30 mm  
378 located at 0.5 mm depth and a mixed-mode defect of the delamination with an additional,  
379 local 75% material degradation. The amplitudes measured along a line across the defects  
380 show high amplitudes in the damaged region and a significant amplitude drop behind the  
381 defective area compared to the baseline measurements on an undamaged part of the plate  
382 (Fig. 9). A reasonable match of the amplitude reduction with the FE simulation results for  
383 0.5 mm delamination depth was found. As observed above, the FE model for a mixed-mode  
384 defect predicts higher amplitudes in the defective region, reasonably matching the  
385 experimental peaks for the two specimens. For the comparison of the angular pattern at the  
386 symmetrical, undamaged location (Fig. 10a), one can observe a reasonably good agreement  
387 between the baseline measurements and FE simulation. The amplitude in the incident wave  
388 direction ( $180^\circ$ ) is about twice the amplitude in the  $0^\circ$  direction, the same amplitude decrease  
389 observed from the line measurements. This matches the experimentally observed amplitude  
390 reduction along a line across the two undamaged plates, which was predicted accurately from  
391 the FE simulation (Fig. 9). The amplitudes are higher along the fiber directions due to the  
392 larger stiffness. For the damage case (Fig. 10b) the incident wave ( $180^\circ$  direction) has a  
393 similar amplitude distribution as the baseline data (Fig. 10a) and no significant back-scattered  
394 amplitude is observed. Both FE simulations predict a decrease in the amplitudes behind the  
395 damage position ( $0^\circ$ ), with some smaller differences in the angular patterns (Fig. 10b).



396

397 **Figure 10** (color online): Comparison between experimental results (baseline and impact  
 398 damage for 2 plates) and FE simulations for delamination (30 mm x 30 mm, 0.5 mm depth)  
 399 and mixed-mode defect (delamination and 75% material degradation): a) undamaged plate;  
 400 b) impact damage; amplitude circular scan; 100 kHz center frequency.

401

402 For the circular measurement around the damage location, it can be seen that both FE results  
 403 provide a good prediction of the experimental observations with reduced forward scattered  
 404 amplitude. The experimental results show a more complicated behavior due the complex  
 405 impact damage and shape. Especially in the 90° direction the measured amplitudes for the  
 406 impact damage in plate 1 are higher than for plate 2 and in the 270° direction, suggesting a  
 407 non-symmetric impact damage. The FE simulations provide a regular pattern compared to  
 408 the experimental results as the impact damage was modelled as a symmetric, rectangular  
 409 delamination with additional decreased stiffness, rather than the actual irregular impact  
 410 shape.

411

412 **VI. CONCLUSIONS**

413 Scattering of the  $A_0$  Lamb wave mode from delaminations in composite plates was  
414 investigated using a 3D FE model. It was shown that the exact delamination shape has only  
415 a small influence on the observed overall scattering pattern. Using a simple damage  
416 implementation in the FE simulations, the effects of delamination size and depth were  
417 investigated. It was demonstrated that the delamination width has a strong influence on the  
418 scattering directivity. The angular scattering pattern indicates the obstruction of the wave  
419 propagation path due to the width of the damaged area and energy trapping within the  
420 delamination. It was found that the angular pattern of the scattered wave field is almost  
421 independent of the delamination length, while the delamination depth has a significant  
422 influence on the magnitude of the scattered waves. The comparison of the FE simulations for  
423 a mixed-mode damage model to measurements for impact damage in two composite plates  
424 showed good agreement. The results show the importance of further investigations of the  
425 three-dimensional scattering characteristics of guided waves at impact damage and  
426 delaminations to improve the detection capability of permanently installed SHM systems for  
427 composite structures.

428

429 **ACKNOWLEDGMENTS**

430 Bibi Intan Suraya Murat gratefully acknowledges funding by the Ministry of Science,  
431 Technology and Innovation (MOSTI), Malaysia and Universiti Teknologi MARA (UiTM),  
432 Malaysia. The authors would like to thank the Composite Systems Innovation Centre,  
433 University of Sheffield, UK for the provision of the composite plates.

434

435 **REFERENCES**

- 436 <sup>1</sup> C. H. Zhong, A. J. Croxford, and P. D. Wilcox, “Remote inspection system for impact  
437 damage in large composite structure,” *Proc. R. Soc. A* **471**, 20140631 (2015).
- 438 <sup>2</sup> H. Y. Choi, H. T. Wu, and F. Chang, “A new approach toward understanding damage  
439 mechanisms and mechanics of laminated composites due to low-velocity impact: Part II-  
440 -analysis,” *J. Compos. Mater.* **25**, 1012–1038 (1991).
- 441 <sup>3</sup> M. O. W. Richardson and M. J. Wisheart, “Review of low-velocity impact properties of  
442 composite materials,” *Compos. Part A* **27**, 1123–1131 (1996).
- 443 <sup>4</sup> A. N. Vorontsov, G. K. Murzakhanov, and V. N. Shchugorev, “Delamination failure of  
444 composite structures,” *Mech. Compos. Mater.* **25**, 723–737 (1990).
- 445 <sup>5</sup> I. G. Scott and C. M. Scala, “A review of non-destructive testing of composite materials,”  
446 *NDT Int.* **15**, 75–86 (1982).
- 447 <sup>6</sup> J. L. Rose, “Ultrasonic guided waves in structural health monitoring,” *Key Eng. Mater.*  
448 **270–273**, 14–21 (2004).
- 449 <sup>7</sup> J. S. Hall and J. E. Michaels, “Multipath ultrasonic guided wave imaging in complex  
450 structures,” *Struct. Health Monit.* **14**, 345–358 (2015).
- 451 <sup>8</sup> C.-T. Ng and M. Veidt, “Scattering of the fundamental anti-symmetric Lamb wave at  
452 delaminations in composite laminates,” *J. Acoust. Soc. Am.* **129**, 1288–1296 (2011).
- 453 <sup>9</sup> M. Castaings and B. Hosten, “Guided waves propagating in sandwich structures made of  
454 anisotropic, viscoelastic, composite materials,” *J. Acoust. Soc. Am.* **113**, 2622–2634  
455 (2003).
- 456 <sup>10</sup> M. J. S. Lowe, G. Neau, and M. Deschamps, “Properties of guided waves in composite  
457 plates, and implications for NDE,” in *Rev. Prog. QNDE* **23**, eds. D. O. Thompson and D.

- 458 E. Chimenti, AIP Conf. Proc. **700**, 214–221 (2004).
- 459 <sup>11</sup> Z. Su, L. Ye, and Y. Lu, “Guided Lamb waves for identification of damage in composite  
460 structures: A review,” J. Sound Vib. **295**, 753–780 (2006).
- 461 <sup>12</sup> S. K. Datta and A. H. Shah, Elastic waves in composite media and structures: with  
462 applications to ultrasonic nondestructive evaluation. CRC Press, Boca Raton (2009).
- 463 <sup>13</sup> N. Guo and P. Cawley, “The interaction of Lamb waves with delaminations in composite  
464 laminates,” J. Acoust. Soc. Am. **94**, 2240–2246 (1993).
- 465 <sup>14</sup> S. Grondel, C. Paget, C. Delebarre, J. Assaad, and K. Levin, “Design of optimal  
466 configuration for generating A(0) Lamb mode in a composite plate using piezoceramic  
467 transducers,” J. Acoust. Soc. Am. **112**, 84–90 (2002).
- 468 <sup>15</sup> M. Castaings, D. Singh, and P. Viot, “Sizing of impact damages in composite materials  
469 using ultrasonic guided waves,” NDT&E Int. **46**, 22–31 (2012).
- 470 <sup>16</sup> P. Guy, Y. Jayet, and L. Goujon, “Guided wave interaction with complex delaminations.  
471 Application to damage detection in composite structures,” Proc. SPIE **5047**, 25–33 (2003).
- 472 <sup>17</sup> C. Ramadas, K. Balasubramaniam, M. Joshi, and C. V Krishnamurthy, “Interaction of  
473 guided Lamb waves with an asymmetrically located delamination in a laminated  
474 composite plate,” Smart Mater. Struct. **19**, 065009 (2010).
- 475 <sup>18</sup> R. Kazys, A. Demcenko, E. Zukauskas, and L. Mazeika, “Air-coupled ultrasonic  
476 investigation of multi-layered composite materials,” Ultrasonics **44**, E819–E822 (2006).
- 477 <sup>19</sup> N. Toyama, J. Noda, and T. Okabe, “Quantitative damage detection in cross-ply laminates  
478 using Lamb wave method,” Compos. Sci. Technol. **63**, 1473–1479 (2003).
- 479 <sup>20</sup> C. H. Wang and L. R. F. Rose, “Wave reflection and transmission in beams containing  
480 delamination and inhomogeneity,” J. Sound Vib. **264**, 851–872 (2003).

- 481 <sup>21</sup> T. Kundu, S. Das, S. A. Martin, and K. V. Jata, “Locating point of impact in anisotropic  
482 fiber reinforced composite plates,” *Ultrasonics* **48**, 193–201 (2008).
- 483 <sup>22</sup> K. Diamanti, J. M. Hodgkinson, and C. Soutis, “Detection of low-velocity impact damage  
484 in composite plates using Lamb waves,” *Struct. Health Monit.* **3**, 33–41 (2004).
- 485 <sup>23</sup> C. B. Pol and S. Banerjee, “Modeling and analysis of propagating guided wave modes in  
486 a laminated composite plate subject to transient surface excitations,” *Wave Motion* **50**,  
487 964–978 (2013).
- 488 <sup>24</sup> O. Mesnil, C. A. C. Leckey, and M. Ruzzene, “Instantaneous wavenumber estimation for  
489 damage quantification in layered plate structures,” *Proc. SPIE* **9064**, 90640D (2014).
- 490 <sup>25</sup> C. T. Ng, M. Veidt, L. R. F. Rose, and C. H. Wang, “Analytical and finite element  
491 prediction of Lamb wave scattering at delaminations in quasi-isotropic composite  
492 laminates,” *J. Sound Vib.* **331**, 4870–4883 (2012).
- 493 <sup>26</sup> D. Singh, R. El Guerjouma, and M. Bentahar, “Interaction of fundamental Lamb modes  
494 with a point impact damaged zone in composite plates,” *Proc. Societe Francaise*  
495 *d’Acoustique, Acoustics 2012*, 2423–2428 (2012).
- 496 <sup>27</sup> C. A. C. Leckey, M. D. Rogge, and F. Raymond Parker, “Guided waves in anisotropic  
497 and quasi-isotropic aerospace composites: three-dimensional simulation and experiment,”  
498 *Ultrasonics* **54**, 385–394 (2014).
- 499 <sup>28</sup> B. I. S. Murat and P. Fromme, “Detection of impact damage in composite panels using  
500 guided ultrasonic waves,” *Proc. SPIE* **8695**, 869506 (2013).
- 501 <sup>29</sup> T. J. Swait, F. R. Jones, and S. A. Hayes, “A practical structural health monitoring system  
502 for carbon fibre reinforced composite based on electrical resistance,” *Compos. Sci.*  
503 *Technol.* **72**, 1515-1523 (2012).

- 504 <sup>30</sup> M. Endrizzi, B.I.S. Murat, P. Fromme, and A. Olivo, “Edge-illumination X-ray dark-field  
505 imaging for visualising defects in composite structures,” *Compos. Struct.* **134**, 895-899  
506 (2015).
- 507 <sup>31</sup> J. Virieux, “P-SV wave propagation in heterogeneous media: Velocity-stress finite-  
508 difference method,” *Geophysics* **51**, 889–901 (1986).
- 509 <sup>32</sup> B. Pavlakovic, M. Lowe, D. Alleyne, and P. Cawley, “DISPERSE: A general purpose  
510 program for creating dispersion curves,” in *Rev. Prog. QNDE* **16**, eds. D. O. Thompson  
511 and D. Chimenti, Plenum, New York, 185–192 (1997).
- 512 <sup>33</sup> T. Hayashi and K. Kawashima, “Multiple reflections of Lamb waves at a delamination,”  
513 *Ultrasonics* **40**, 193-197 (2002).
- 514 <sup>34</sup> J. S. Hall, P. Fromme, and J. E. Michaels, “Guided Wave Damage Characterization via  
515 Minimum Variance Imaging with a Distributed Array of Ultrasonic Sensors,” *J.*  
516 *Nondestruct. Eval.* **33**, 299-308 (2014).
- 517 <sup>35</sup> H. Sohn, D. Dutta, J. Y. Yang, H. J. Park, M. DeSimio, S. Olson, and E. Swenson,  
518 “Delamination detection in composites through guided wave field image processing,”  
519 *Compos. Sci. Technol.* **71**, 1250–1256 (2011).
- 520